PCCP

Accepted Manuscript

ROYAL SOCIETY OF CHEMISTRY

www.rsc.org/pccp

Cite this: DOI: 10.1039/c0xx00000x

www.rsc.org/xxxxxx

ARTICLE TYPE

Sulfate-ion-assisted galvanic replacement tuning of silver dendrites to highly branched chains for effective SERS

Yunxia Zhang, Shaodong Sun, Xiaozhe Zhang, Linli Tang, Xiaoping Song and Zhimao Yang*

Received (in XXX, XXX) Xth XXXXXXXXX 20XX, Accepted Xth XXXXXXXXX 20XX

DOI: 10.1039/b000000x

Morphology is a primary part of designing metal nanocrystals and nanomaterials with controlled functional properties. Here, we demonstrate the potential of foreign sulfate ions to tune the silver dendrites to highly branched chains through a simple galvanic replacement reaction without introducing any organic surfactants. We further illustrate the underlying mechanism according to diffusion-limited aggregation (DLA) in the presence of sulfate ions. The special aspects of this simple synthetic strategy are the control of both the nucleation process and the subsequent crystal growth stage by using sulfate ions as the ionic surfactants thereby tuning the total surface energies on various crystal facets in solution and transforming crystal growth habits of the products. Moreover, the highly branched silver chains (HBSCs) with pure surfaces have been successfully employed as a Raman probe for surface-enhanced Raman spectroscopic (SERS) analysis of rhodamine 6G (R6G). The particular morphology of those HBSCs also makes them find potential applications in biosensing, catalysis and optics.

1. Introduction

The synthesis of metal nanocrystals with controllable complex morphologies is a key goal in modern materials science and has attracted substantial interests in recent years,[1,2] because they often exhibit unusual chemical, physical, electronic, optical, magnetic and catalytic properties showing great promise in many applications.[3,4] Among various metal nanostructures, branched nanocrystals with self-assembled and hierarchical architectures are increasingly fascinating due to their unique structures, physicochemical properties and numerous applications in catalysis,[5] surface enhanced Raman scattering (SERS),[6,7] plasmon routers,[8] photothermal therapy[9] and so on.

To date, a variety of electrochemical, wet chemical and physical strategies have produced diverse metal branched nanocrystals such as palladium flowers,[5] Pt–Ni bimetallic nanobundles,[10] urchin-like silver nanowires,[11] Au/Pd bimetallic multipods,[12] gold dendrites[13] and so forth. Shape-directing agents have been included in general tool bench as potential morphology drivers of metal branched nanocrystals due to their significant roles in determining the final shapes.[12-17] Usually, strong organic surfactants/polymers such as cetyltrimethylammonium bromide (CTAB) or poly(vinylpyrrolidone) (PVP) could differentially bind to the crystal faces of a growing crystal thus stabilize and block its growth to achieve the branched nanostructures with desired shape and size.[14,15] For instance, palladium tetrapods[16] and nanostars[17] could be successfully constructed by solution-phase synthesis using PVP or CTAB as stabilizers or reducing agent, respectively. Besides, inorganic surfactants are of great importance for obtaining metal branched nanocrystals and have been demonstrated to be good alternatives of strong organic surfactants for metal morphology control.[14,18-20] Many metal ions (cobalt,[14] iron,[20] tungsten,[21] chromium[22] and silver[23] ions) have been proved to be efficient directors of Pt nanostructures by manipulating nucleation and growth rate of the nanocrystals in different crystallographic directions. Copper[24] and aluminium[25] ions have been also used to facilitate the growth of silver nanowires and copper selenide nanocubes, respectively. Additionally, there are some examples on the use of negative ions such as fluorine,[26] sulfate[27] or chloride[28] ions to prepare silver micro/nanostructures. In many cases, these inorganic ions did not incorporate in the metal nanostructures and were not detected on the surface or within the final nanostructures. They just poisoned or enhanced the growth of crystal facets[18,19] or decelerated the reaction process by altering the reduction kinetics through redox reaction between the foreign molecules and metal nanoparticles.[14,20]

However, the organic surfactants used for morphology control might strongly adsorb on the surfaces of products introducing the heterogeneous impurities or significant interference thus limit some special applications such as SERS, biosensing, catalysis and so on.[12,13,16] And most of the previous studies on the use of inorganic surfactants to metal morphology control also have to cooperate with the organic surfactants (PVP[18-20,23,24] and hexadecylamine[25]), solvents (ethylene glycol[18,24,28], octadecene[25], oleic acid and oleylamine[21,22]) or reducing agents (hexadecanediol[14]). Furthermore, those strategies assisted by inorganic surfactants were focused on metal polyhedrons since the polyhedral metal nanocrystals might lead to catalytic selectivity in chemical reaction resulting in enhanced catalytic and electrocatalytic performances.[14,18,20-22] Then, inorganic surfactant such as foreign ions could also be utilized as shape directors of branched metal nanostructures without any organic additives for more applications. Although a few hierarchical silver dendrites have been achieved with the assistance of

fluorine[26] or sulfate[27] ions, the underlying growth mechanism of the metal branched nanocrystals is needed to be clarified. Furthermore, the previous report[27] only describes the morphological changes of silver products induced by the sulfate ions, but the detailed functions of the foreign ions during the growth process are also still not clearly understood.

In our previous work, icker-like silver architectures with numerous branches were obtained via a simple replacement reaction assisted by an external magnetic field.[29] And the external magnetic field might redistribute the surface energies of different crystallographic facets where aggregation of silver atoms and nanoparticles could be disturbed. Herein, we demonstrate the potential of foreign sulfate ions to tune the silver dendrites to similar highly branched chains through a galvanic replacement reaction without introducing any organic surfactants. The special aspects of this simple synthetic strategy are the control of both the nucleation process and the subsequent crystal growth stage by using sulfate ions as the ionic surfactants thereby tuning the total surface energies on various crystal facets in solution and transforming crystal growth habits of the products. A possible mechanism for the highly branched silver chains (HBSCs) growth is suggested according to diffusion-limited aggregation (DLA) in the presence of sulfate ions. Furthermore, these HBSCs with pure surfaces have been successfully applied to enhance the Raman scattering signals of rhodamine 6G (R6G), and the particular morphology will make them find potential applications in biosensing, catalysis and optics.

2. Experimental details

2.1. Chemicals and Reagents

Commercial zinc foil (> 99.99%) was purchased from Shanghai Longxin Chemical Industry Co., Ltd (Shanghai, China). Silver nitrate (> 99.8%) was obtained from Tianjin Tian Gan Chemical Industry Technology development Co., Ltd (Tianjin, China). Anhydrous sodium sulfate, potassium sulfate and sodium nitrate (> 99.0%) were from Tianjin Hengxing Chemical Preparation Co., Ltd (Tianjin, China). All the chemicals were of analytical grade and used as purchased without further purification. Water was purified by a UPH-I-5T water purification system (Ulupure, Chengdu Ultrapure Technology co., Ltd, Chengdu, China). Doubly deionized distilled (DDI) water was used unless otherwise stated.

2.2. Synthesis

Zinc foil was cut into 5 × 1 cm^2 pieces and rubbed with fine sandpaper then rinsed with water, acetone, dilute hydrochloric acid and ethanol in sequence to remove the contaminations. The solutions (4 ml) containing 10 mM Ag^+ and different foreign ions (Na^+, K^+, SO_4^{2-}, NO_3^-) with various concentrations were prepared using analytically pure $AgNO_3$, Na_2SO_4, K_2SO_4 and $NaNO_3$ as well as deionized water. Particularly, the mixed solution turned to be a little turbid due to the formation of Ag_2SO_4 after the SO_4^{2-} ions were added to the $AgNO_3$ solution. But the mixed solution would shortly restore clear because the concentration of Ag^+ ions was 10 mM resulting in a maximum Ag_2SO_4 concentration of 5 mM which was less than the maximum concentration of Ag_2SO_4 (~ 25.6 mM) in aqueous solution at room temperature (20 °C) and ambient pressure.[30] To deposit silver products, the zinc foils were immersed into the above mixed solutions for a period of time, respectively. After the reaction, the products were thoroughly washed with deionized water and ethanol, dried and collected for characterization.

2.3 Characterization

The silver products were characterized with field emission scanning electron microscopy (FE-SEM, JSM-7000F, JEOL Inc., Japan) at an accelerating voltage of 20 kV. The Energy dispersive X-ray (EDX) analysis was obtained with an Oxford INCA EDX detector installed on the JEOL JSM-7000F. The transmission electron microscopy (TEM) and high resolution transmission electron microscopy (HRTEM) analysis as well as selected-area electron diffraction (SAED) pattern analysis were performed on a JEOL JEM-2100 transmission electron microscope operating at an accelerating voltage of 200 kV. Samples for TEM analysis were prepared by ultrasonic dispersion for 5 min with ethanol (2 mL) in a 3 mL centrifuge tube. Then, the products were dropped onto a carbon-coated copper grid and dried in air before TEM analysis. The X-ray diffraction measurement was carried out with a Bruker-AXS D8-Advance X-ray diffractometer using Cu K_α (λ=1.54 Å) radiation from 35° to 80°. The X-ray photoelectron spectra (XPS) were recorded by X-ray photoelectron spectroscopy (England, Kratos Axis Ultra DLD) using an Al mono Kα X-ray source. All the peaks were corrected with the C 1s peak at 286.4 eV as the reference.

2.4 SERS measurements

The SERS measurements were carried out on a confocal microprobe Raman spectrometer (Jobin-YVon HR800) with an excitation wavelength of 633 nm and power of 0.05 mW. The probed area was about 1 μm in diameter with a 100×microscope objective lens and the typical spectrum acquisition time was 1 s. In order to precisely acquire the SERS spectra of the HBSCs and silver dendrites, identical amount of the collected silver products were sufficiently dispersed into equal volume of ethanol through the ultrasonic dispersing technology, respectively. Then, a few of the above mixtures (200 μl) were homogeneously dispersed onto different Si wafers (0.5 × 0.5 cm^2) and dried in air, respectively. The SERS spectra were recorded after immersing the Si wafers covered by the as-synthesized silver products into R6G solutions (in ethanol) for 24 h, rinsing with ethanol and drying in air at room temperature and ambient pressure.

3. Results and discussions

3.1 Characterization

In the present investigation, a low-magnification SEM image of the as-obtained silver products reveals that the resulting silver architecture is one-dimensional (1D) chain consisting of many short secondary branches that are oriented to their own long trunks (Fig. 1a). Fig. 1b is a typical high-magnification SEM image of the HBSCs indicating that some secondary branches have developed into several shorter (20 - 200 nm) ones stretching in random directions, respectively. All the diffraction peaks observed in Fig. 1c are indexed to the (111), (200), (220) and (311) diffraction peaks of the face-centered cubic Ag (JCPDS no. 04-0783). Furthermore, the corresponding composition analysis by EDX spectroscopy (Fig. 1d) also displays that the composition of the sample is silver crystal. XPS is a well-known technique for determining the surface elemental composition of a solid such as its oxidation state and/or chemical environment. In order to investigate the stability of the as-obtained HBSCs, the XPS spectrum was measured to uncover the surface oxidation state of

HBSCs. Fig. S1 depicts the XPS spectrum of the HBSCs, where peaks of Ag 3d, O 1s, C 1s, Zn 2p and Si 2p can be identified. According to the position of Ag 3d core level peak, it is obvious that the Ag (I) oxidation state (368.2 eV) exists in the metal silver (374.2 eV), suggesting the presence of the impurity of the Ag_2O. Additionally, the Si 2p core level peak centered at 100.1 eV corresponds to the Si substrate contribution during the XPS measurements. And the weak Zn 2p core level peak centered at 1021.8 eV and O 1s core level peak centered at 529.4 eV could be ascribed to the Zn^{2+} and O^{2-} contributions, respectively.[31] Therefore, it is deduced that a small fraction of Zn was oxidized to ZnO but the sulfate ions did not attach on the silver crystal surfaces during the reaction process. Furthermore, it also demonstrates that a few surface Ag was oxidized to Ag_2O during the sample drying and handling under normal ambient conditions.

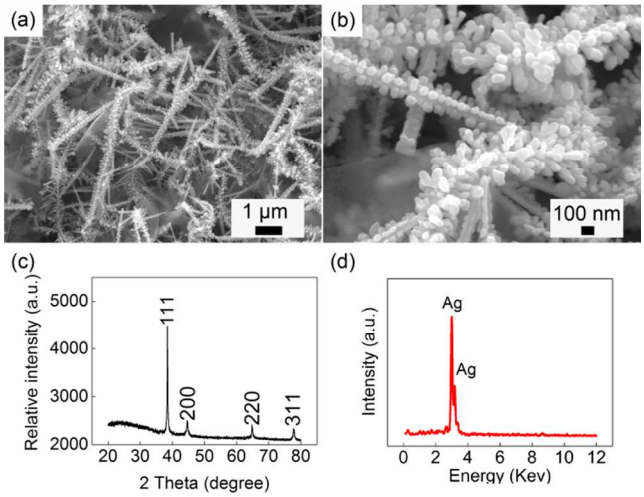

Fig.1 (a) Low-magnification and (b) magnified SEM images as well as (c) and (d) corresponding XRD pattern and EDX spectrum of the HBSCs obtained in 10 mM $AgNO_3$ aqueous solution in the presence of 2.5 mM Na_2SO_4 at a reaction time of 10 min.

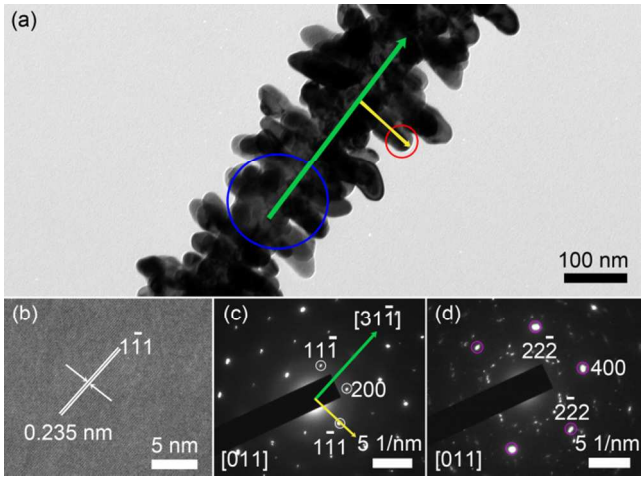

Fig. 2 (a) TEM image of the HBSCs in Fig. 1a and (b) HRTEM image of the red circled area as well as (c) and (d) SAED patterns of the red and blue circled areas in Fig. 2a, respectively.

A representative TEM image of the HBSCs is depicted in Fig. 2a. It is also found that a number of short branches alternately arrange oriented to a trunk in diverse directions and each branch is made up of small nanoparticles that are "cemented" together. Fig. 2b is a typical HRTEM image of an individual branch, and the lattice fringe of about 0.235 nm is marked by white lines and arrows corresponding to (111) facets of cubic phase of Ag crystals. Furthermore, the corresponding SAED pattern (Fig. 2c) presents a single crystal nature indexed to the cubic phase of silver viewed along the [011] zone axis. It can be explained by the natural tendency for the nanoparticles to favor oriented attachment[32,33] and the known atomic reorganization occurring during the growth and subsequent evolution.[34] Actually, the SAED pattern of the local trunk in the blue circle consists of several overlapped single crytal patterns and one of the single SAED patterns is also indexed to the [011] zone axis diffraction based on the corresponding analysis of the diffraction spots circled by purple rings in Fig. 2d. It could be ascribed to the highly branched morphology of the silver architectures where many branches have grown oriented to the trunk in a variety of directions and some ones even have evolved into several smaller branches leading the branches to sit on top of one another (Fig. 1b). On the basis of the aforementioned results, it is credible that the highly branched silver chain with <311>-oriented trunk and some <111>-oriented branches are successfully achieved.

3.2 Morphological evolution and growth mechanism

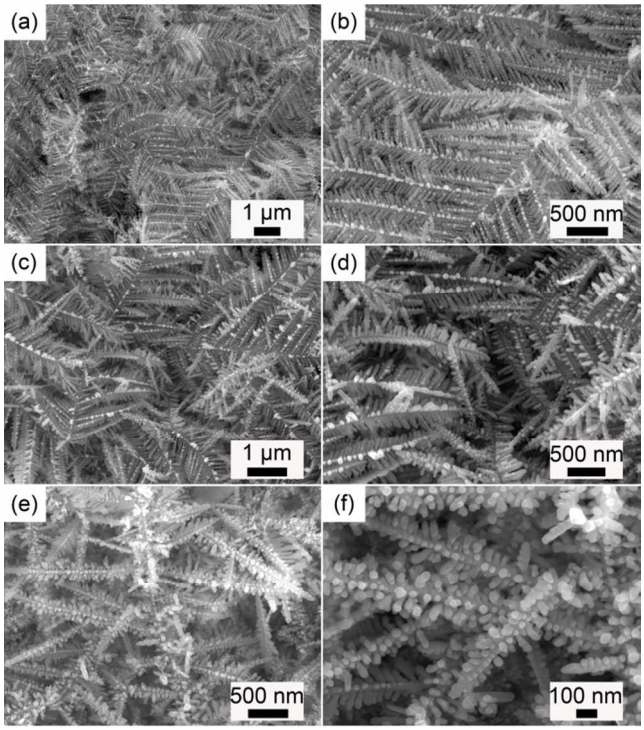

Fig. 3 Typical SEM images of the silver products prepared with the $AgNO_3$ concentration of 10 mM, growth time of 15 min and different foreign inorganic additives: (a) 0 mM foreign ions, (c) 2.5 mM $NaNO_3$ and (e) 2.5 mM K_2SO_4, respectively. (b), (d) and (f) are the magnified SEM images of (a), (c) and (e), respectively.

Various foreign ions might exercise a great influence on the morphology evolution of the silver products in this reaction system (Fig. 3). Common silver dendrites were only observed in the presence of $AgNO_3$ solution without any foreign ions (Fig. 3a and b). Upon the addition of Na_2SO_4 into the $AgNO_3$ solution, the

products displayed extremely different 1D silver architectures with lots of short branches (Fig. 1a) demonstrating that the foreign ions (Na^+ and SO_4^{2-} ions) might have played a key role in modifying the morphology of the silver products. Obviously dendritic silver products were also formed (Fig. 3c and d) indicating that the Na^+ ions might hardly alter the crystal growth habit and general appearance of the silver products when the foreign addition was adjusted from Na_2SO_4 to $NaNO_3$ while carefully keeping other reaction parameters the same. Thus, the SO_4^{2-} ions were highly believed to have dominated the morphology evolution of the silver products in the present work. An additional piece of evidence supporting this notion was the observation of similar HBSCs attained by switching the foreign addition to K_2SO_4 (2.5 mM), which further clearly proved the drastic effects of the SO_4^{2-} ions in the formation and assembly process of the silver nanoparticles to be grown HBSCs during this reaction system (Fig. 3e and f).

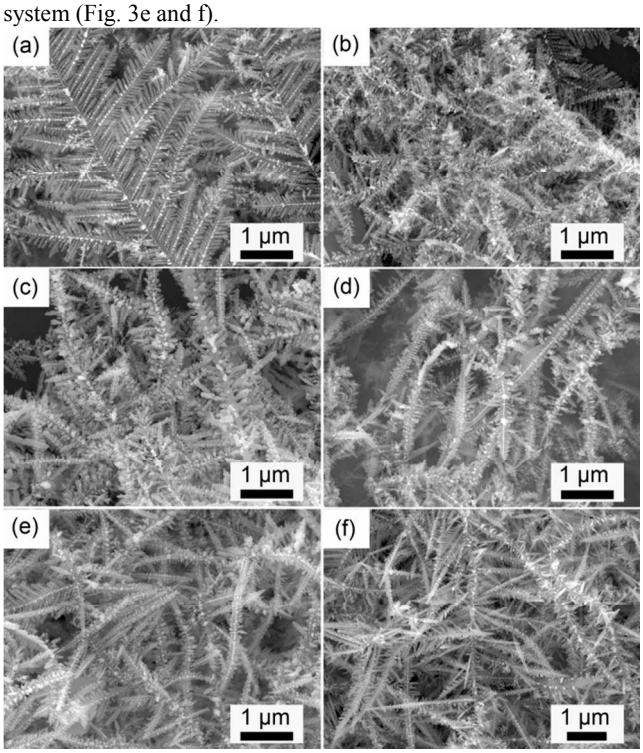

Fig. 4 SEM images of silver products obtained with the Ag^+ ion concentration of 10 mM and different reaction times and concentrations of SO_4^{2-} ions: (a)-(d) 10 min, 1 mM, 1.5 mM, 5 mM and 15 mM as well as (e) and (f) 20 min, 30 mM and 50 mM, respectively.

Fig. 4 details the morphology evolution of the silver products depending on various concentrations of the foreign SO_4^{2-} ions. Ordinary silver dendrites still formed as before with the SO_4^{2-} ion concentration increasing to 1 mM (Fig. 4a). The products kept occupying dendritic appearances but no long secondary or tertiary branches when the SO_4^{2-} ion concentration was further increased to 1.5 mM (Fig. 4b). The dendritic morphology started to alter as the amount of SO_4^{2-} ion was enhanced to 2.5 mM (Fig. 1a), and the silver architectures represented well-defined exterior assembled by numerous short branches arranging oriented to a long trunk. Subsequently, such similar HBSCs with much larger diameters were obtained with the increase of SO_4^{2-} ion concentration and reaction time (Fig. 4c-f). Interestingly, it was found that some longish secondary branches of the HBSCs also followed an identical growth pattern of the main trunk exhibiting smaller branches around the sub-trunk line. Thus, the presence of SO_4^{2-} ions at sufficiently high concentrations (Fig. 1a, 3e, 3f and 4d-f) would cause the nanoparticles to take on pronounced transform of growth habit and assembly process for the resultant silver products. Furthermore, the SO_4^{2-} ions could not work on every silver atom and nanoparticles thereby generating a handful of silver dendrites during this nonequilibrium reaction system.

Additionally, to examine the growth mechanism of those HBSCs, the SEM images were taken for their growth at different time intervals (Fig. 5). The silver products with a short growth time of 30 s (Fig. 5a) appeared large clusters composed of numerous tiny nanoparticles. When the growth time was increased to 2 min, nanoparticle-aggregated clusters dominated by longitudinal growth developed from the formed large clusters (Fig. 5b). Many small nanoparticles have preferentially assembled to plentiful cells which might be the desirable and critical starting points for the formation of HBSCs. Then, the previously generated cells grew longer and quickly developed into long 1D architectures with relatively short branches in various directions oriented to the trunk as time passed (Fig. 5c, 1a and 3f). In particular, the silver products exhibited broken dendrites instead of HBSCs for the longer growth time. Frequently, the fractal growth of dendritic nanostructures has been explained by DLA model involving a single cluster to which additional monomers diffuse from the bulk solution and attach once they reach a site adjacent to the edge of the cluster during the diffusive processes in nonequilibrium systems.[35] And the DLA model has provided much useful insight into the formation of some dendritic nanostructures such as silver fractal dendrites,[36] nanoparticles clusters,[37] dendritic flowers[38] and so forth. Therefore, the formation of some broken dendrites in this study might be attributed to the accessibility of a minimum total surface free energy[39] for the fresh nanoparticles to attach on the neighbouring branches upon gradual decrease of the supersaturation of the reaction system resulted from consumption of the silver ions, which might facilitate the formation of dendrites because of the DLA model.

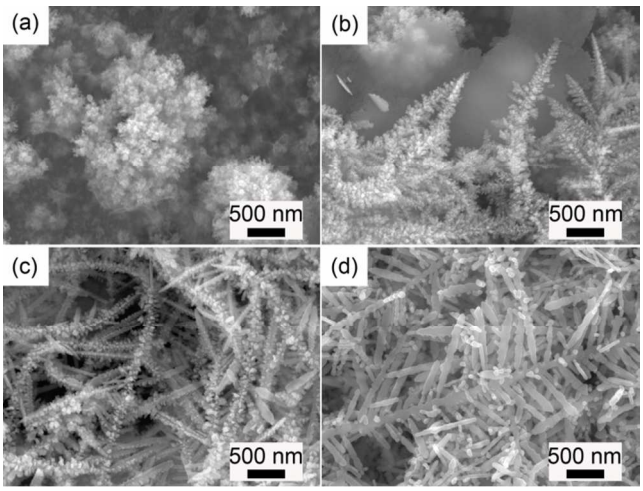

Fig. 5 SEM images of the silver products synthesized with the Ag^+ and SO_4^{2-} ion concentrations of 10 mM and 2.5 mM, respectively as well as different reaction times: (a) 30 s, (b) 2 min, (c) 3 min and (d) 20 min.

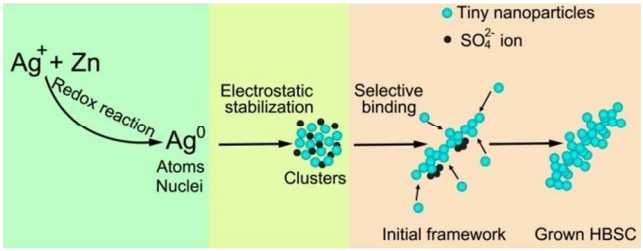

Fig.6 Schematic illustration of the formation process of HBSCs assisted by foreign SO_4^{2-} ions.

Based on the experiments above, a plausible formation process is speculated as shown in Fig.6. In this approach, the electron transfer, nucleation and growth coexist simultaneously and can be simply achieved via the reduction of Ag^+ ions by Zn foil at room temperature. Since the standard electrode potential of the Ag^+/Ag pair ($E^\circ_{Ag+/Ag}$ = +0.799 V) is larger than that of Zn^+/Zn pair ($E^\circ_{Zn+/Zn}$ = - 0.762 V),[30] then the galvanic replacement reaction will take place as follows:

$$Zn + 2Ag^+ \rightarrow 2Ag + Zn^{2+} \quad (1)$$

When a Zn foil is positioned into an $AgNO_3$ aqueous solution with some SO_4^{2-} ions, the Ag^+ ions are rapidly reduced to form silver atoms by electron transfer with simultaneous release of Zn^{2+} ions into the solution. Once the concentration of silver atoms has reached the supersaturation level, they will begin to nucleate. Then, a wealth of silver nuclei will instantaneously form at random positions in the reaction system due to the diffusion of silver atoms and increasingly aggregate together to be nanoparticles. At the same time, the nucleation process can be pronouncedly influenced by inorganic ions because of their relatively small sizes associated with nuclei.[40] As a result, the SO_4^{2-} ions are likely to coordinate to silver nuclei and adsorb onto the surfaces of silver nanoparticles thereby stabilizing them against aggregation through electrostatic stabilization[28,41,42] which could sufficiently retard the silver particle growth. Therefore, numerous tiny nanoparticles did not fuse to lager nanoparticles but only aggregated to be clusters (Fig. 5a). With prolonging of the reaction duration, the existing silver nanoparticles would still self-assemble to nanostructures or a chain-like network as shown in Fig.5b. The chain-like network will still exhibit dendritic morphology with relatively long trunk and short branches in terms of surface-energy minimization once the particle has reached a critical value[43] through DLA model.[35] Generally, additives such as impurities or capping agents are believed to be operative for altering the order of free energies of different facets through their interactions with the specific facets of a nanocrystal in a solution-phase synthesis.[44] This transformation may significantly affect the relative growth rates of different facets and result in nanocrystals with different morphologies.[40,44,45]Then, the SO_4^{2-} ions might also serve as the ionic surfactants like in previous synthesis[18,19,46] and prefer interacting with some crystal facets of the established dendritic framework by binding strongly to them thus reduce the corresponding surface energies and block these crystal facets from adding freshly Ag atoms and nanoparticles. Accordingly, the subsequent Ag atoms and nanoparticles have to seek other crystal facets disliking SO_4^{2-} ions to attain an optimal organization to minimize the total surface free energy.[40] It might dominate the nucleation and growth rate in different crystallographic directions and dilute the influences of DLA model resulting in the formation of these silver HBSCs. Obviously, the SO_4^{2-} ions have shown dislike to the {311} crystal facets but appeared to favor the {111} crystal facets of silver architectures thereby facilitating the longitudinal growth of the silver architectures but weaken the extending of branches. Despite these reasonable explanations, much more efforts are still needed to be devoted to exploring exact roles of SO_4^{2-} ions during the nucleation, growth and assemble of silver nanoparticles and growth of architectures.

3.3 Surface enhanced Raman scattering

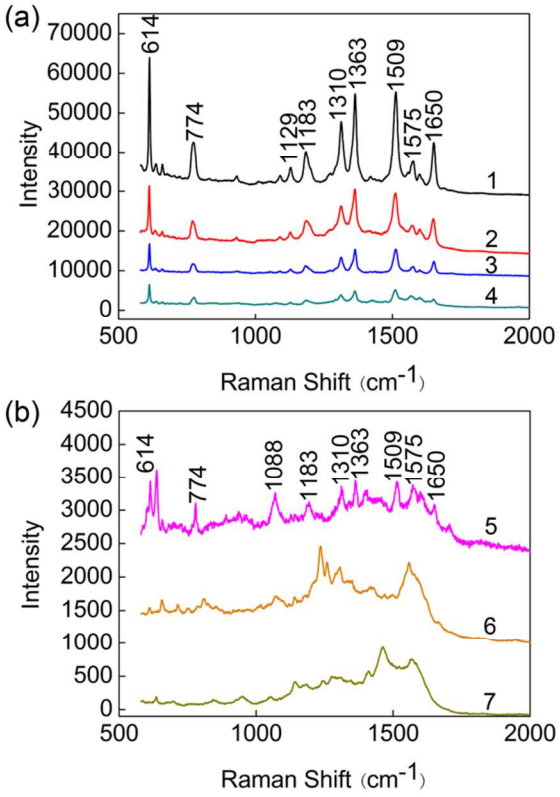

Fig. 7 Raman spectra of HBSCs (curve 1) and silver dendrites (curve 2) with 1×10^{-4} M R6G as well as HBSCs with different R6G concentrations: 1×10^{-5} M (curve 3), 1×10^{-6} M (curve 4), 1×10^{-7} M (curve 5), 1×10^{-8} M (curve 6) and 1×10^{-9} M (curve 7).

SERS has previously been utilized as a powerful analytical tool for detecting chemical information of molecule adsorbed on the surface of metal nanostructures.[47-52] In general, the SERS measurement is highly depending on the exterior morphology and surface structure of the substrate. Compared with the dendrites of closely aligned branches which might weaken the SERS signal amplifications, the HBSCs might be a promising candidate for SERS application due to their specific morphology and surface structure which provide many opportunities for most of the Raman signals coming from the molecules adsorbed on the surface of the silver architectures. In the present study, R6G has been chosen as the molecule probe because of its large scattering cross section. A comparison of the spectra recorded from the active substrates of HBSCs (curve 1) and silver dendrites (curve 2) indicates that the former has achieved prominently stronger enhancement of the Raman signal for R6G than that of silver dendrites (Fig. 7). UV visible spectra of nanostructures are

strongly dependent on the morphology and therefore surface plasmon resonance (SPR) property of nanostructures.[53] Fig. S2 shows the UV-visible spectra of the as-obtained silver dendrites and HBSCs suspended in ethanol. It is observed that the silver dendrites present two absorption peaks at 350 nm and 430 nm, respectively, while the HBSCs had broad absorptions ranging from about 410 nm to near-infrared which could be attributed to the SPR properties depending on the highly branched morphology.[54] Corrections between SERS and SPR have been studied and connected theoretically and experimentally.[55, 56] And it has been proved that optimizing the correlation between the SPR of the substrate and the excitation wavelength provides an efficient way to increase the SERS performance.[57] Then, the peculiar morphology with broad absorptions might display LSPR (Localized Surface Plasmon Resonance) over a broad range of wavelength and strong enhancement of the electromagnetic field at the sharp corners and edges of the HBSCs.[58, 59] Especially, numerous nanogaps formed by overlapped branches affording high density of "hot spots" trapping the analyst to generate significant Raman enhancement.[60-62] Specifically, the observed Raman bands that are assigned to R6G include C–C–C in-plane bending (614 cm^{-1}), C–H out-plane bending (774 cm^{-1}), C–H in-plane bending (1129 and 1183 cm^{-1}), C–O–C stretching (1310 cm^{-1}) and C–C stretching of the aromatic ring (1363, 1509, 1575 and 1650 cm^{-1}) on basis of the reported literature.[62,63]

It is difficult to estimate the intrinsic SERS enhancement factor (EF) due to the difficulties of obtaining many variables such as adsorbed molecules, laser scattering volume and so on.[64] Thus, the analytical enhancement factor (AEF) has been adopted to estimate the SERS performance of those HBSCs, which is defined by the following equation:[64]

$$\mathrm{AEF} = \frac{I_{\mathrm{SERS}}/C_{\mathrm{SERS}}}{I_{\mathrm{RS}}/C_{\mathrm{RS}}} \qquad (2)$$

where I_{SERS} can be achieved from a SERS-active substrate (Si wafer covered by HBSCs) with a R6G concentration of C_{SERS} and I_{RS} denotes the Raman intensity of R6G solution with a concentration of C_{RS} (Fig. S3). In the studies, all spectra were normalized for the acquisition time with all of the other identical parameters including the laser wavelength, laser power, microscopic magnification and spectro-meter. Then, the AEF of the band at 614 cm^{-1} has been evaluated to be approximately 10^6 for those HBSCs, which is sufficient for the observation of single molecule SERS signals revealing that the HBSCs can be used as effective SERS substrate in trace detection.[64] Furthermore, the SERS spectra of a series of concentrations of R6G on the HBSCs (Fig. 7) demonstrate that some weak Raman signals could still be measured from the samples, even the concentration has been decreased to 10^{-8} M (curve 6) and as low as to 10^{-9} M (curve 7) showing the high sensitivity of the HBSCs which might be used as a "fingerprint" for the detection of R6G.[65] In addition, it has been also observed that a logarithmic plot between the peak intensity of the 614 cm^{-1} band and the R6G concentration has yielded a good linear relationship over a wide concentration range, as shown in Fig.8. Similar observations were reported for R6G SERS detection using silver nanowires[66] and nanosheet[67] films. It also suggests that the HBSCs substrate could potentially be used for quantitative SERS analysis of the molecules of interest. Due to their satisfying SERS performances, such HBSCs serving as great substrates is promising candidate for detecting other trace biomolecules or dangerous chemicals.[68]

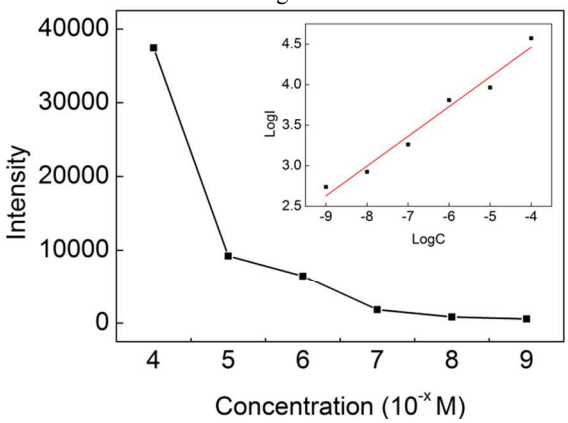

Fig.8 The relationship of peak intensities at 614 cm^{-1} and concentrations of R6G (the inset is the linear relationship between the logarithmic intensities and concentrations of R6G).

4. Conclusion

In conclusion, we have represented the potential of foreign sulfate ions to reshape the silver dendrites to highly branched chains through a galvanic replacement reaction without introducing any organic surfactants. The special aspects of this simple synthetic strategy are the control of both the nucleation process and the subsequent crystal growth stage by using sulfate ions as the ionic surfactants thereby tuning the total surface energies on various crystal facets in solution and transforming crystal growth habits of the products. A possible mechanism for the highly branched silver chains (HBSCs) growth is suggested based on diffusion-limited aggregation in the presence of sulfate ions. Furthermore, these HBSCs with pure surfaces have been successfully applied to enhance the Raman scattering signals of R6G, and the particular morphology will make them find potential applications in biosensing, catalysis and optics.

Acknowledgements

This work was supported by National Science Foundation of China (NSFC Nos. 51272209 and 51302213), National Key Technology Research and Development Program of the Ministry of Science and Technology of China (No. 2012BAE06B08), Program for Key Science and Technology Innovative Research Team of Shaanxi Province (No. 2013KCT-05), Youth Foundation of Shaanxi Province of China (No. 2012JQ6007), Doctoral Fund of Ministry of Education of China (No. 20120201120051) and the Fundamental Research Funds for the Central Universities.

Notes and references

School of Science, State Key Laboratory for Mechanical Behavior of Materials, MOE Key Laboratory for Non-Equilibrium Synthesis and Modulation of Condensed Matter, Collaborative Innovation Center of Suzhou Nano Science and Technology, Xi'an Jiaotong University, Xi'an, 710049, ShaanXi, People's Republic of China. Fax/Tel: +86 2982665995; E-mail: zmyang@mail.xjtu.edu.cn

† Electronic Supplementary Information (ESI) available: The Raman spectra of R6G (1×10^{-2} M in ethanol) solution (Fig. S1). See DOI: 10.1039/b000000x/

1 M. Rycenga, C. M. Cobley, J. Zeng, W. Li, C. H. Moran, Q. Zhang, D. Qin and Y. Xia, *Chem. Rev.*, 2011, **111**, 3669-3712.
2 B. Lim and Y. Xia, *Angew. Chem. Int. Ed.*, 2011, **50**, 76-85.
3 S. Sun and Z. Yang, *RSC Adv.*, 2014, **4**, 3804-3822.
4 Y. Xia, Y. Xiong, B. Lim and S. E. Skrabalak, *Angew. Chem. Int.*

Ed., 2008, **48**, 60-103.
5 J. Watt, S. Cheong, M. F. Toney, B. Ingham, J. Cookson, P. T. Bishop and R. D. Tilley, *ACS nano*, 2010, **4**, 396-402.
6 H. Chen, P. Kannan, L. Guo, H. Chen and D. Kim, *J. Mater. Chem.*, 2011, **21**, 18271-18278.
7 X. Zou, E. Ying and S. Dong, *Nanotechnology*, 2006, **17**, 4758.
8 Y. Fang, Z. Li, Y. Huang, S. Zhang, P. Nordlander, N. J. Halas and H. Xu, *Nano lett.*, 2010, **10**, 1950-1954.
9 B. Van de Broek, N. Devoogdt, A. D Hollander, H. Gijs, K. Jans, L. Lagae, S. Muyldermans, G. Maes and G. Borghs, *ACS nano*, 2011, **5**, 4319-4328.
10 Z. Niu, D. Wang, R. Yu, Q. Peng and Y. Li, *Chem. Sci.*, 2012, **3**, 1925-1929.
11 W. Hsiao, H. Chen, Y. Yang, Y. Chen, C. Lee and H. Chiu, *ACS appl. Mater. interfaces*, 2011, **3**, 3280-3284.
12 L. F. Zhang, S. L. Zhong and A. W. Xu, *Angew. Chem. Int. Ed.*, 2013, **52**, 645-649.
13 W. Jia, J. Li and L. Jiang, *ACS appl. Mater. Interfaces*, 2013, **5**, 6886-6892.
14 S. I. Lim, I. Ojea-Jiménez, M. Varon, E. Casals, J. Arbiol and V. Puntes, *Nano lett.*, 2010, **10**, 964-973.
15 V. F. Puntes, K. M. Krishnan and A. P. Alivisatos, *Science*, 2001, **291**, 2115-2117.
16 R. Zhao, G. Fu, T. Zhou, Y. Chen, X. Zhu, Y. Tang and T. Lu, *Nanoscale*, 2014, **6**, 2776-2781.
17 A. Kedia and P. S. Kumar, *J. Phys. Chem. C*, 2012, **116**, 1679-1686.
18 T. Herricks, J. Chen and Y. Xia, *Nano Lett.*, 2004, **4**, 2367-2371.
19 H. Song, F. Kim, S. Connor, G. A. Somorjai and P. Yang, *J. Phys. Chem. B*, 2005, **109**, 188-193.
20 B. Lim, X. Lu, M. Jiang, P. H. Camargo, E. C. Cho, E. P. Lee and Y. Xia, *Nano lett.*, 2008, **8**, 4043-4047.
21 J. Zhang and J. Fang, *J. Am. Chem. Soc.*, 2009, **131**, 18543-18547.
22 R. Loukrakpam, P. Chang, J. Luo, B. Fang, D. Mott, I. Bae, H. R. Naslund, M. H. Engelhard and C. Zhong, *Chem. Commun*., 2010, **46**, 7184-7186.
23 M. E. Grass, Y. Yue, S. E. Habas, R. M. Rioux, C. I. Teall, P. Yang and G. A. Somorjai, *J. Phys. Chem. C*, 2008, **112**, 4797-4804.
24 K. E. Korte, S. E. Skrabalak and Y. Xia, *J. Mater. Chem.*, 2008, **18**, 437-441.
25 W. Li, R. Zamani, M. Ibáñez, D. Cadavid, A. Shavel, J. R. Morante, J. Arbiol and A. Cabot, *J. Am. Chem. Soc.*, 2013, **135**, 4664-4667.
26 W. Ye, Y. Chen, F. Zhou, C. Wang and Y. Li, *J. Mater. Chem.*, 2012, **22**, 18327-18334.
27 S. Xie, X. Zhang, D. Xiao, M. C. Paau, J. Huang and M. M. Choi, *J. Phys. Chem. C*, 2011, **115**, 9943-9951.
28 S. H. Im, Y. T. Lee, B. Wiley and Y. Xia, *Angew. Chem.*, 2005, **117**, 2192-2195.
29 Y. Zhang, S. Sun, X. Zhang, L. Tang, X. Song, B. Ding and Z. Yang, *Chem. Eng. J.*, 2014, **240**, 494-502.
30 W. M. Haynes, D. R. Lide and T. J. Bruno, *CRC Handbook of Chemistry and Physics (Internet Version)*, CRC/Taylor and Francis Press, Boca Raton, FL, 94th edn, 2014.
31 J. F. Moulder, W. F. Stickle, P. E. Sobol and K. D. Bomben, *Handbook of X-ray Photoelectron*, Perkin-Elmer Corporation Press, Eden Prairie, Minnesota, 1992.
32 J. F. Banfield, S. A. Welch, H. Zhang, T. T. Ebert and R. L. Penn, *Science*, 2000, **289**, 751-754.
33 K. Cho, D. V. Talapin, W. Gaschler and C. B. Murray *J. Am. Chem. Soc.*, 2005, **127**, 7140-7147.
34 H. Zheng, R. K. Smith, Y. Jun, C. Kisielowski, U. Dahmen and A. P. Alivisatos, *Science*, 2009, **324**, 1309-1312.
35 R. M. Brady and R. C. Ball, *Nature*, 1984, **309**, 225-229.
36 X. Qin, Z. Miao, Y. Fang, D. Zhang, J. Ma, L. Zhang, Q. Chen and X. Shao, *Langmuir*, 2012, **28**, 5218-5226.
37 F. Gentile, M. L. Coluccio, A. Toma, E. Rondanina, M. Leoncini, F. D. Angelis, G. Das, C. Dorigoni, P. Candeloro and E. D. Fabrizio, *Microelectron. Eng.*, 2012, **98**, 359-362.
38 A. L. Swatek, Z. Dong, J. Shaw Jr and M. R. Islam, *J. Exp. Nanosc.*, 2010, **5**, 10-16.
39 J. W. Mullin, *Crystallization*, Butterworth-Heinemann Press, London, 3rd edn, 1997.
40 B. Wiley, T. Herricks, Y. Sun and Y. Xia, *Nano Lett.*, 2004, **4**, 1733-1739.
41 C. A. Mirkin, *Inorg. Chem.*, 2000, **39**, 2258-2272.
42 S. Lin, Y. Tsai, C. Chen, C. Lin and C. Chen, *J. Phys. Chem. B*, 2004, **108**, 2134-2139.
43 L. D. Marks, *Rep. Prog. Phys.*, 1994, **57**, 603-649.
44 M. H. Kim, B. Lim, E. P. Lee and Y. Xia, *J. Mater. Chem.*, 2008, **18**, 4069-4073.
45 C. Burda, X. Chen, R. Narayanan and M. A. El-Sayed, *Chem. Rev.*, 2005, **105**, 1025-1102.
46 X. Teng and H. Yang, *Nano lett.*, 2005, **5**, 885-891.
47 W. J. Cho, Y. Kim and J. K. Kim, *ACS Nano*, 2012, **6**, 249-255.
48 A. Gutés, C. Carraro and R. Maboudian, *J. Am. Chem. Soc.*, 2010, **132**, 1476-1477.
49 M. J. Mulvihill, X. Y. Ling, J. Henzie and P. Yang, *J. Am. Chem. Soc.*, 2010, **132**, 268-274.
50 S. Nie and S. R. Emory, *Science*, 1997, **275**, 1102-1106.
51 S. Shanmukh, L. Jones, J. Driskell, Y. Zhao, R. Dluhy and R. A. Tripp, *Nano Lett.*, 2006, **6**, 2630-2636.
52 D. Sun, G. Zhang, X. Jiang, J. Huang, X. Jing, Y. Zheng, J. He and Q. Li, *J. Mater. Chem. A*, 2014, **2**, 1767-1773.
53 N. Felidj, J. Aubard, G. Levi, J. R. Krenn, M. Salerno, G. Schider, B. Lamprecht, A. Leitner and F. R. Aussenegg, *Phys. Rev. B*, 2002, **65**, 075419.
54 J. Sharma, Y. Tai and T. Imae, *J. Phys. Chem. C*, 2008, **112**, 17033-17037.
55 M. Moskovits, *Rev. Mod. Phys.*, 1985, **57**, 783-826.
56 R. Alvarez-Puebla,, B. Cui, J.-P. Bravo-Vasquez, T. Veres and H. Fenniri, *J. Phys. Chem. C*, 2007, **111**, 6720-6723.
57 J. B. Jackson and N. J. Halas, *Proc. Natl. Acad. Sci. U.S.A.*, 2004, **101**, 17930-17935.
58 X. Zou and S. Dong, *J. Phys. Chem. B*, 2006, **110**, 21545-21550.
59 I. Pastoriza-Santos and L. M. Liz-Marzan, *J. Mater. Chem.*, 2008, **18**, 1724-1737.
60 M. K. Kinnan and G. Chumanov, *J. Phys. Chem. C*, 2007, **111**, 18010-18017.
61 M. Wang, J. Hu, Y. Li and E. S. Yeung, *Nanotechnology*, 2010, **21**, 145608.
62 Y. Yang, Z. Li, K. Yamaguchi, M. Tanemura, Z. Huang, D. Jiang, Y. Chen, F. Zhou and M. Nogami, *Nanoscale*, 2012, **4**, 2663-2669.
63 P. Hildebrandt and M. Stockburger, *J. Phys. Chem.*, 1984, **88**, 5935-5944.
64 E. C. Le Ru, E. Blackie, M. Meyer and P. G. Etchegoin, *J. Phys. Chem. C*, 2007, **111**, 13794-13803.
65 Q. Huang and X. Zhu, *Mater. Chem. and Phys.*, 2013, **138**, 689-694.
66 C. Chen, J. Hao, L. Zhu, Y. Yao, X. Meng, W. Weimer and Q. K. Wang, *J. Mater. Chem. A*, 2013, **1**, 13496-13501.
67 T. Gao, Y. Wang, K. Wang, X. Zhang, J. Dui, G. Li, S. Lou and S. Zhou, *ACS appl. mater. Interfaces*, 2013, **5**, 7308-7314.
68 M. Zhang, A. Zhao, H. Sun, H. Guo, D. Wang, D. Li, Z. Gan, W. Tao, *J. Mater. Chem.*, 2011, **21,** 18817-18824.